MATHEMATICAL DETAILS OF THE REFRACTION-BASED COMPUTED TOMOGRAPHY

Anton Maksimenko
Photon Factory, Institute of Materials Structure Science,
High Energy Accelerator Research Organization (KEK),
1-1 Oho, Tsukuba, Ibaraki 305-0801, Japan
email: antonmx@post.kek.jp

Tetsuya Yuasa
Faculty of Engineering,
Yamagata University Yonezava, Yamagata 992, Japan.

Masami Ando
Photon Factory, Institute of Materials Structure Science,
High Energy Accelerator Research Organization (KEK),
1-1 Oho, Tsukuba, Ibaraki 305-0801, Japan

ABSTRACT
In recent publications we have presented method for the computed tomography reconstruction from the X-ray refraction contrast. It was shown that the method has many advantages over conventional absorption contrast-based tomography. However, those papers were mainly dedicated to the experimental realization of the technique and the results of the reconstruction while the details of the mathematical algorithm were left out of consideration. Although the mathematical formalism used for the algorithm is very similar to the well developed Filtered Back Projection method, it has important peculiarities which do not allow the adoption of the currently present algorithms. Thus, the material of this paper concentrates on the originally developed mathematical algorithm of the CT-reconstruction from the refraction contrast (i.e. the information on the x-ray refraction after penetration through the object). It also includes the gradient-to-field transformation method applicable in the context of the algorithm.

KEY WORDS
computed tomography, refraction contrast, X-ray, reconstruction algorithm

1 Introduction

The X-ray computed tomography (CT) reconstruction [1, 2] of the inner structure of an object is very powerful tool for the nondestructive observations. Since the development in early 1970's it has found numerous applications in many fields of science, technology and medicine. Most of the methods which utilize the principal scheme of the CT are based on the X-ray absorption contrast. In the recent years X-ray imaging techniques were rapidly developing and provided a user with different types of contrast which may be preferable in a certain conditions and have important advantages over the absorption contrast (see Refs.[3, 4, 5, 6, 7, 8, 9, 10] for example). One of these contrasts is the so called refraction contrast [9, 10, 3, 11, 12, 13, 14]. Generally speaking, it can be any type of the x-ray image with the intensity distribution being a function of the refraction angle. Main advantages of this contrast are the possibility to observe tiny cracks and deformations invisible in other types of contrasts (what makes it highly applicable in technology and structure science) and better sensitivity to the low Z materials (which is of great importance in medical imaging) [12, 14, 13, 15]. The CT-reconstruction based on the refraction contrast[16, 15, 17, 18, 19, 20, 21, 22, 23] was expected to possess the same advantages. In the recent publications [16, 15, 22, 23] we have presented implementation of this idea and demonstrated how it works in experiment. The results of the reconstruction of the experimental data proved the expectations. However, the mathematical and computational details of the reconstruction process were described briefly in the experimentally-oriented works while they have some peculiarities which does not allow to apply the absorption-based CT algorithm and software to the refraction case. Therefore this paper is mainly dedicated to the mathematical aspects of the problem, emphasizing the difference between CT algorithms for the absorption and refraction cases.

2 Theory

As it was mentioned above, the refraction contrast is the distribution of the X-ray intensity dependent on the deflection angle of the X-ray beam penetrated through an object. In most cases this contrast is a mixture of the absorption and refraction contrasts. Fortunately there are well described methods which can extract the information on the refraction angle distribution from the mixture of the contrasts [12, 13, 24]. Due to this fact we assume here that the information on the deflection angle is extracted without considering how it was done. The deflection angle of the x-ray beam penetrated through an object is calculated as the integral over the beam path with the elemental deflection as the integrand[12, 17, 20, 18]:

$$\Delta\alpha = \int_S \frac{\partial\widetilde{n}(\mathbf{r})}{\partial t}\, ds, \tag{1}$$

where $\widetilde{n}(\mathbf{r})$ has a relation to the refraction index $n(\mathbf{r})$ as $\widetilde{n} = 1 - n$, $\mathbf{r} \equiv (x, y)$ since we utilize the plane geometry of the common CT model (see fig.1). As it is shown in fig.2, t is the coordinate in the diffraction plane that is perpendicular to the beam-vector. In this integral the X-ray path inside the object S can be approximated by the straight line due to small deviation of the refractivity from unity in the X-ray region: $\widetilde{n} \leq 10^{-5}$. The subintegral function in eq.(1) can be used in form $\partial\widetilde{n}(\mathbf{r})/\partial t = \nabla\widetilde{n}(\mathbf{r}) \cdot \mathbf{t} = |\nabla\widetilde{n}(\mathbf{r})| \cos(\angle\nabla\widetilde{n}(\mathbf{r}), \mathbf{t})$, where $\mathbf{t}$ is the unit vector along the t axis with the x and y components $\mathbf{t} = (\sin\Theta, -\cos\Theta)$. In accordance with the geometry depicted in fig.2 the angle $\angle\nabla\widetilde{n}(\mathbf{r}), \mathbf{t} = \Theta - \varphi(\mathbf{r}) + \pi/2$, where angles Θ and $\varphi(\mathbf{r})$ give the directions of the X-ray beam and the gradient of the refraction index field $\nabla\widetilde{n}(\mathbf{r})$ respectively. Then we can rewrite eq.(1) as follows:

$$\Delta\alpha = \int_S |\nabla\widetilde{n}(\mathbf{r})| \sin(\Theta - \varphi(\mathbf{r}))\, ds. \qquad (2)$$

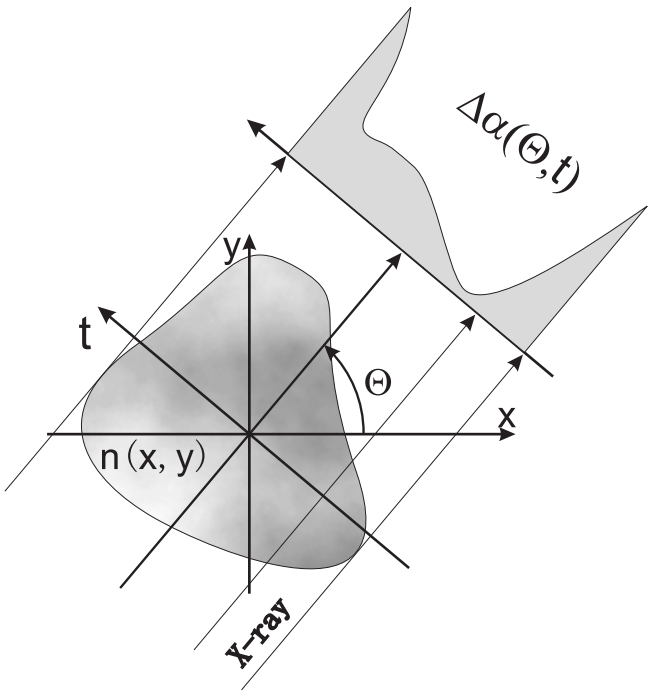

Figure 1. Basic CT geometry. Here Θ is the angle between axis x and the beam-vector. $\Delta\alpha(\Theta, t)$ is the projection with the information about the deflection angle.

The equation (2) is not enough for the CT-reconstruction because it has two unknown functions: absolute value of the gradient $|\nabla\widetilde{n}|$ and its direction given by the angle φ. The missing equation comes from the fact that the integral of the tangential component of the gradient $\nabla\widetilde{n}(\mathbf{r})$ is equal to the difference of the field in starting and finishing points of the integration. And since the values of the field $\widetilde{n}$ are equal on the both sides of the object, the difference between them has always zero value:

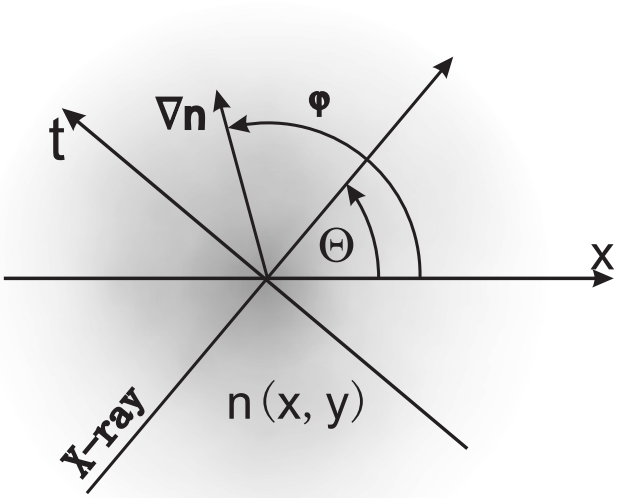

Figure 2. To the calculation of the deflection angle $\Delta\alpha$. Please note that the angle between the X-ray beam and the gradient $\nabla\widetilde{n}(\mathbf{r})$ is equal to $\varphi(\mathbf{r}) - \Theta$.

$$0 = \int_S |\nabla\widetilde{n}(\mathbf{r})| \cos(\Theta - \varphi(\mathbf{r}))\, dr. \qquad (3)$$

In order to write the equation which can serve as the base for the CT-reconstruction we need to multiply eq.(2) by the complex unity i and add it to the eq.(3):

$$i\Delta\alpha = \int_S |\nabla\widetilde{n}(\mathbf{r})| e^{i(\Theta - \varphi(\mathbf{r}))}\, dr. \qquad (4)$$

The component $e^{i\Theta}$ can be factored from the integral and moved to the left part of the equation since $\Theta = const$ over the integration path:

$$i\Delta\alpha e^{i\Theta} = \int_S |\nabla\widetilde{n}(\mathbf{r})| e^{i\varphi(\mathbf{r})}\, dr.. \qquad (5)$$

According to the general CT method [2], one needs to acquire the information on the deflection angle as a function of the angular position of the object and space coordinate (respectively Θ and t in fig.1): $\Delta\alpha(\Theta, t)$. Eq.(5) written for the case of the rotation position Θ serves as the base for the CT-reconstruction:

$$i\Delta\alpha(\Theta, t) e^{i\Theta} = \int_{S(\Theta,t)} |\nabla\widetilde{n}(\mathbf{r})| e^{i\varphi(\mathbf{r})}\, dr. \qquad (6)$$

Here the integration paths $S(\Theta, t)$ is approximated by the straight line $x\cos\Theta + y\sin\Theta = t$. One can note that this equation is very similar to the equation for the absorption-contrast based CT reconstruction. The difference is in the input functions (they are $i\Delta\alpha(\Theta, t)e^{i\Theta}$ for the refraction

case and $-\log\left(I(\Theta,t)/I_0\right)$ for the absorption) and the functions to be reconstructed ($|\nabla\widetilde{n}(\mathbf{r})|e^{i\varphi(\mathbf{r})}$ and $\mu(\mathbf{r})$ for the refraction and absorption cases respectively). However, there is one important difference between these cases. In the equation for the absorption-based CT both input and output functions are in the real number space while the refraction-based CT utilizes the functions in the complex number space. This means that the absorption-based CT algorithms can not be adopted for the refraction case and the problem requires its own original algorithm and software.

Due to the structure of the eq.(6), the mathematical formalism of the refraction-based CT algorithm is the same that is used for the absorption case (so called Filtered Backprojection method). Basically, it consists of four steps. i) Fourier transform of the sinogram $\Delta\alpha(\Theta,t)$:

$$P_\Theta(w)=\int_{-\infty}^{\infty}\Delta\alpha(\Theta,t)e^{-2\pi iwt}dt. \tag{7}$$

ii) Filtering of the transformed function $P_\Theta(w)$:

$$S_\Theta(w)=P_\Theta(w)b(w). \tag{8}$$

Here $b(w)$ is a filtering function. There are lot of filtering functions used in the CT-reconstruction (in the ideal case $b(w)\equiv 1$, so-called Ramp filter). However the filters usually used in the absorption-based CT are hardly applicable in refraction case because all of them suppress high frequency components emphasizing low frequency ones. It is reasonable in case of absorption contrast because most useful information is contained in the low domain while high components mostly consist of noise. Contrastingly, in the refraction case higher Fourier components play important role and should not be suppressed by the filtering function. iii) Backward Fourier transform of the filtered function:

$$Q_\Theta(t)=\int_{-\infty}^{\infty}S_\Theta(w)|w|e^{2\pi itw}dw. \tag{9}$$

The resulting function $Q_\Theta(t)$ is known as the filtered sinogram. Please note that in the above equations (7)-(9) we omitted the member $ie^{i\Theta}$ since all integrations are performed at constant Θ. iv) Backprojecting of the filtered sinogram to the real space:

$$|\nabla\widetilde{n}(\mathbf{r})|e^{i\varphi(\mathbf{r})}=i\int_0^{\pi}Q_\Theta(t)e^{i\Theta}d\Theta. \tag{10}$$

Or in the vector form:

$$\nabla\widetilde{n}(\mathbf{r})=\int_0^{\pi}Q_\Theta(t)\mathbf{t}(\Theta)d\Theta, \tag{11}$$

This algorithm is presented for the continuous form of the equations. In any practical application the function $\Delta\alpha(\Theta,t)$ is known only in a certain points Θ_m and t_n. Therefore the discrete form of the algorithm, described in Ref.[2], must be used in actual calculations.

The refraction-based CT equation (6) shows that the reconstructed function is the gradient $\nabla\widetilde{n}(\mathbf{r})$, while most users would prefer the results in terms of the real physical value $\widetilde{n}(\mathbf{r})$ rather than its gradient. In order to calculate it, one can perform CT-reconstruction and then build $\widetilde{n}(\mathbf{r})$ from $\nabla\widetilde{n}(\mathbf{r})$ using the property of the scalar field gradient

$$\widetilde{n}(\mathbf{r_0})=\int_{\infty}^{\mathbf{r_0}}\nabla\widetilde{n}(\mathbf{r})d\mathbf{r}. \tag{12}$$

However, the basic equality $\nabla\times(\nabla\widetilde{n}(\mathbf{r}))\equiv 0$ is not fulfilled strictly due to the computational error in step (iv) of the CT-reconstruction algorithm (see eq.(11)). This means that the value of the $\widetilde{n}(\mathbf{r_0})$ depends on the choice of the integration path so that one needs to calculate more than one integral (12) along different trajectories and then use the average of them as the most realistic result. In order to avoid this problem we used another way to reconstruct the value $\widetilde{n}$. We can write the eq.(12) with the gradient from the eq.(11) and change the order of the integrations:

$$\widetilde{n}(\mathbf{r_0})=\int_0^{\pi}d\Theta\int_{\infty}^{\mathbf{r_0}}Q_\Theta(t)\mathbf{t}(\Theta)d\mathbf{r}. \tag{13}$$

The inner integration can be performed over the t axis since the integration path over $\mathbf{r}$ can be chosen arbitrary. Denoting this inner integral, which can be called "integrated" sinogram, as

$$\widehat{Q}_\Theta(t)=\int_{\infty}^{t}Q_\Theta(\tau)d\tau, \tag{14}$$

we can finally write

$$\widetilde{n}(\mathbf{r})=\int_0^{\pi}\widehat{Q}_\Theta(t)d\Theta. \tag{15}$$

In other words, the gradient-to-field conversion can be done before the backprojecting of the filtered sinogram. This conversion 'builtin' inside the reconstruction algorithm has certain advantages over the conversion performed after the reconstruction. First of all, the inner integral in eq.(14) is one-dimensional contrastingly to the integral (12) which is performed over a curve on the surface (x,y). This makes the integration mathematically easier and computationally cheaper. Secondary, the equality $\nabla\times(\nabla\widetilde{n}(\mathbf{r}))\equiv 0$ holds true strictly before the fourth step of the algorithm due to the member $|w|$ in the integrand of the eq.(9) which guarantees the mean value of the function $Q_\Theta(t)$ to be equal to zero.

At this point the reasonable question may appear: why in the eq.(1) don't we take the derivative $\partial/\partial t$ out of the integral and perform the integration over t before the reconstruction process:

$$\widehat{\alpha}(\Theta,t)\equiv\int_{-\infty}^{t}\Delta\alpha(\Theta,\tau)d\tau=\int_S\widetilde{n}(\mathbf{r})\,ds. \tag{16}$$

This equation has the form of classical CT problem (considering $\widehat{\alpha}(\Theta,t)$ and $\widetilde{n}(\mathbf{r})$ as input and unknown functions

respectively) and currently available algorithms for the CT reconstruction can manage it since both components are in real number space. However, the integration over t in the left part of the eq.(16) is performed using experimentally acquired data which holds certain measurement error. This error accumulates while integrating so that the value of the integral may significantly differ from zero at the edge of the image. This accumulated error breaks the necessary condition for the CT algorithms which assume that the value of the input function ($\widehat{\alpha}(\Theta, t)$ in our case) are the same on the both sides of the region of interest (width of the images). Similar approach was presented in Ref.[19] proving these expectations: the accumulated error may be clearly seen in the right part of the fig.2b of the mentioned work[19] as the white stripes outside the object where black intensity may is expected. After the reconstruction (see fig.3a in Ref.[19]) these stripes lead to the dark ark on the left side of the image as well as adding additional contrast to the image itself. Therefore the function $\widehat{\alpha}(\Theta, t)$ may not be directly used as the input to the CT algorithms. Also it is necessary to note that the filtering windows often used in the CT algorithms cannot reduce this problem. Moreover the filters are hardly applicable in this approach since the frequency domain of the $\widehat{\alpha}(\Theta, t)$ function has different meaning. Perhaps some non-trivial mathematical manipulations may help to solve the problem, but they also add the complexity to the method and therefore we think that the approach purposed in this paper is preferable.

3 Results

The algorithm presented above can be tested with some simulated data. This simulated data, due to its ideality, do not include noise, experimental error and any portion of other contrasts. All these elements are always present in any real experimentally acquired data and after the reconstruction it is difficult to distinguish which of the artifacts in the resulting images comes from the experiment and which one are brought by the reconstruction algorithm. Therefore the simulated data are preferable in the context of this paper. We have chosen the object for simulation consisting of 4 circles with different values of the refractivity. The object itself is shown in fig.3a and the summary of the information about every element of the object (radius, position, and the refraction index) is presented in Table 1. In data simulation

Table 1. Information on the simulated object. All sizes in the table are given in the relative units. In this units radius of the reconstruction area is equal to 1.0.

number of the element	1	2	3	4
radius of the circle	0.85	0.4	0.3	0.2
x of the center	-0.1	0.2	-0.5	-0.1
y of the center	0.0	0.0	0.3	-0.6
normalized refraction index $\widetilde{n}$	0.5	1.0	0.6	0.7

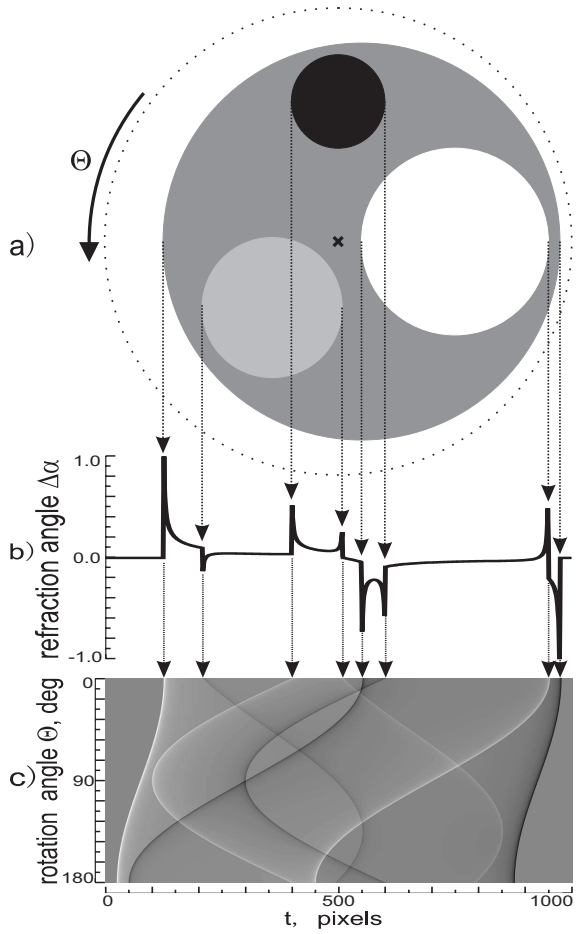

Figure 3. a) The object chosen for the data simulation. Dotted circle shows the reconstruction region with center denoted by "$\times$" mark. b) The deflection angle as the function of the space coordinate t at the rotation position $\Theta = 0$. The deflection angle is normalized to the maximum deflection which depends on the value of the refraction index field. c) Simulated sinogram (function $\Delta\alpha(\Theta, t)$) of the object.

we used number of pixels 1000 what is a reasonable number since in the nowadays most of the CCD cameras have resolution of this order. Number of the rotation angles Θ we set the same 1000. This is also adequate number especially for the high-intensity X-ray sources. One can note that in this simulated object the X-ray deflect only on the boundaries between the elements. Then the deflection of the X-ray penetrated through this simulated object can be easily calculated. The simulated map of the deflection angle is shown in fig.3b for one rotation position $\Theta = 0$ as a function of the space coordinate t: $\Delta\alpha(\Theta = 0, t)$. Fig.3c represents the sinogram $\Delta\alpha(\Theta, t)$ in form of 2D grayscale map.

As it was described in the theoretical part, the sinogram shown in fig.3c is the input function to the CT-reconstruction algorithm. The filtered sinogram $Q_\Theta(t)$

which is the result of the steps i-iii of the algorithm is depicted in fig.4a. Finally, after the backprojection of the filtered sinogram to the real space we can obtain the gradient of the refraction index field $\nabla\widetilde{n}(\mathbf{r})$ which is shown in fig.5 as two 2D maps representing the absolute value of the gradient and its direction (figures 5a and 5b respectively). The gray circles of different intensities in fig.5a has clear interpretation: the gradient of the refraction index field on the boundaries between the elements is described by the delta-function multiplied by the coefficient proportional to the difference of the refraction index. After the discretization of the equations this delta-function turns to the peak function of the limited width. Exactly these peaks on the boundaries between the elements are observed in fig.5a. Fig.5b can be the same easily interpreted taking into account the fact that the direction of the gradient is perpendicular to the boundary of the elements and directed from toward the region with larger refractivity.

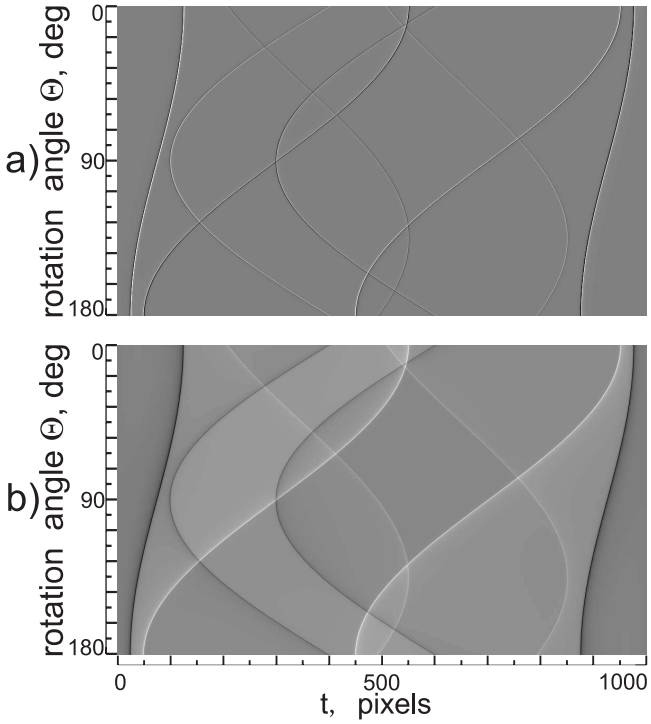

Figure 4. Filtered sinogram $Q_\Theta(t)$ (a) and the "integrated" sinogram after the gradient-to-field transformation $\widetilde{Q}_\Theta(t)(b)$.

Although the structure of the object can be understood from the pictures in fig.5, they are not the realistic visualization of the object shown in fig.3a since they represent the gradient of the refraction index field while the object represents the field itself. The gradient-to-field transformation described above (see eq.(13)) results in the integrated sinogram shown in fig.4b. Backprojecting this sinogram to the real space brings the desired 2D map of the refractivity $\widetilde{n}(\mathbf{r})$. It is depicted in fig.6. The comparison of this figure with the original object shows very good correspondence.

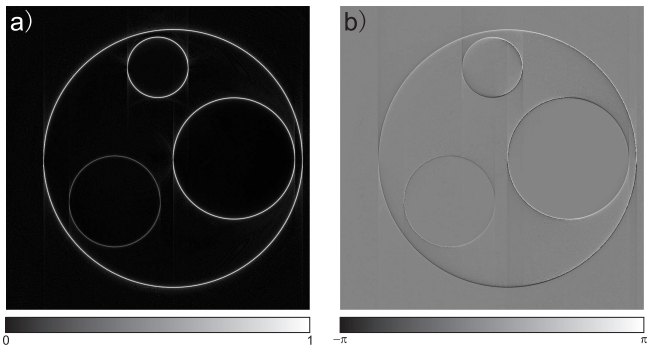

Figure 5. Result of the reconstruction of the simulated data by the algorithm without the 'builtin' gradient-to-field transformation: a) the absolute value of the gradient $|\nabla\widetilde{n}(\mathbf{r})|$ and b) the direction of the gradient in form $\varphi(\mathbf{r})|\nabla\widetilde{n}(\mathbf{r})|$.

The shapes of the elements are reconstructed with the accuracy of 3 pixels and the values of the refractivity are within 5% error.

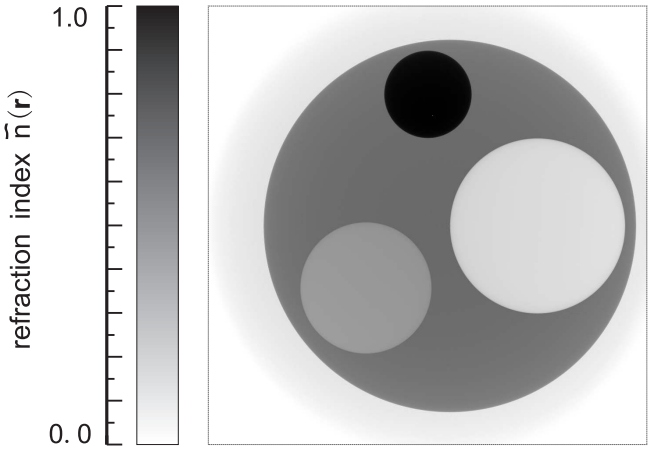

Figure 6. Result of the reconstruction of the simulated data by the algorithm with the 'builtin' gradient-to-field transformation.

Finally we can say that the problem of the mathematically correct algorithm for the CT-reconstruction from the X-ray refraction contrast was solved. The software prepared on the base of this algorithm tested on the simulated data showed very good accordance with the expectations, what validates the applicability of the method and proves the adequacy of the physical model. Also original method of the gradient-to-field conversion was presented. This computationally cheap method provided very accurate results.

References

[1] G N Hounsfield. Computerized transverse axial scanning (tomography). 1. description of system. *Brit. J. Rad.*, 46:1016–1022, 1973.

[2] A C Kak and Malcolm Slaney. *Principles of Computerized Tomographic Imaging*. Society of Industrial and Applied Mathematics, 2001.

[3] P Cloetens, W Ludwig, J Baruchel, D Van Dyck, J Van Landuyt, J P Guigay, and M Schlenker. Holotomography: Quantitative phase tomography with micrometer resolution using hard synchrotron radiation x rays. *Appl. Phys. Let.*, 75(19):2912–2914, 1999.

[4] T J Davis, D Gao, T E Gureyev, A W Stevenson, and S W Wilkins. Phase-contrast of weakly absorbing materials using hard x-rays. *Nat.*, 373:595–598, 1995.

[5] T J Davis, T E Gureyev, D Gao, A W Stewenson, and S W Wilkins. X-ray image contrast from a simple phase object. *Appl. Phys. Lett.*, 74(16):3173–3176, 1995.

[6] U Bonse and M Hart. An x-ray interferometer. *Appl. Phys. Lett.*, 6:155–156, 1965.

[7] Atsushi Momose, Tohoru Takeda, Yuji Itai, and Keiichi Hirano. Phasecontrast xray computed tomography for observing biological soft tissues. *Nat. Med.*, 2:473–475, 1996.

[8] Atsushi Momose. Phase-contrast x-ray imaging based on interferometry. *J. of Synch. Rad.*, 9:136–142, 2002.

[9] Keiichi Hirano, Anton Maksimenko, Hiroshi Sugiyama, and Masami Ando. X-ray optics for observing dark-field and bright-field refraction-contrast images. *Jap. J. Appl. Phys.*, 41:L595–L598, 2002.

[10] Alberto Bravin. Exploiting the x-ray refraction contrast with an analyser: the state of the art. *J. Phys. D: Appl. Phys.*, 36(10A):A24–A29, 2003.

[11] V N Ingal and E A Beliaevskaya. X-ray plane-wave topography observation of the phase contrast from a non-crystalline object. *J. Phys. D: Appl. Phys.*, 28:2314–2317, 1995.

[12] D Chapman, W Thomlinson, R E Johnston, D Washburn, E Pisano, N Gmür, Z Zhong, R Menk, F Arfelli, and D Sayers. Diffraction enhanced x-ray imaging. *Phys. Med. Biol.*, 42(11):2015–2025, 1997.

[13] Miles N Wernick, Oliver Wirjadi, Dean Chapman, Zhong Zhong, Nikolas P Galatsanos, Yongyi Yang, Jovan G Brankov, Oral Oltulu, Mark A Anastasio, and Carol Muehleman. Multiple-image radiography. *Phys. Med. Biol.*, 48(23):3875–3895, 2003.

[14] Masami Ando, Anton Maksimenko, Hiroshi Sugiyama, Wanwisa Pattanasiriwisawa, Kazuyuki Hyodo, and Chikao Uyama. Simple x-ray dark- and bright-field imaging using achromatic laue optics. *Jap. J. Appl. Phys.*, 41:L1016–L1018, 2002.

[15] Anton Maksimenko, Masami Ando, Hiroshi Sugiyama, and Eiko Hashimoto. Possibility of computed tomographic reconstruction of cracks from x-ray refraction contrast. *Jap. J. Appl. Phys.*, 44(20):L633–L635, 2005.

[16] Anton Maksimenko, Masami Ando, Hiroshi Sugiyama, and Tetsuya Yuasa. Computed tomographic reconstruction based on x-ray refraction contrast. *Appl. Phys. Lett.*, 86:124105–124107, 2005.

[17] F A Dilmanian, Z Zhong, B Ren, X Y Wu, L D Chapman, I Orion, and W C Thomlinson. Computed tomography of x-ray index of refraction using the diffraction enhanced imaging method. *Phys. Med. Biol.*, 45:933–946, 2000.

[18] K M Pavlov, C M Kewish, J R Davis, and M J Morgan. A variant on the geometrical optics approximation in diffraction enhanced tomography. *J. Phys. D: Appl. Phys.*, 34:A168–A172, 2001.

[19] I Koyama, Y Hamaishi, and A Momose. Phase tomography using diffraction-enhanced imaging. In *Eighth International Conference on Synchrotron Radiation Instrumentation*, volume 705 of *AIP Conf. Proc.*, pages 1283–1286, 2004.

[20] M Wernick, J Brankov, D Chapman, Y Yang, C Muehleman, Z Zong, and M A Anastasio. A preliminary study of multiple-image computed tomography. In *Developments in X-Ray Tomography IV*, volume 5535 of *Proc. SPIE*, page 369, 2004.

[21] Jovan G Brankov, Miles N Wernick, Yongyi Yang, Jun Li, Carol Muehleman, Zhong Zhong, and Mark A Anastasio. Multiple-image computed tomography. *Med. Phys.*, 33:278, 2006.

[22] Anton Maksimenko, Eiko Hashimoto, Masami Ando, Hiroshi Sugiyama, and Tetsuya Yuasa. First attempt of the medical application of the refraction-based computed tomography. In *Medical Imaging 2006: Physics of Medical Imaging*, volume 6142 of *Proc. of the SPIE*, pages 1263–1266, 2006.

[23] E Hashimoto, A Maksimenko, H Sugiyama, K Hyodo, D Shimao, T Yuasa, Y Nishino, T Ishikawa, K Mori, Y Arai, K Hirano, and M Ando. First application of x-ray refraction based computed tomography to a biomedical object. In *Medical Imaging 2006: Physics of Medical Imaging*, volume 6142 of *Proc. of the SPIE*, pages 369–372, 2006.

[24] Anton Maksimenko. Modified diffraction enhanced imaging method. *in review*.